Evolution of shallow groundwater flow systems in areas of degrading permafrost

Bense, V.F.; Ferguson, G.; Kooi, H.

published in
Geophysical Research Letters
2009

DOI (link to publisher)
10.1029/2009GL039225

document version
Publisher's PDF, also known as Version of record

GEOPHYSICAL RESEARCH LETTERS, VOL. 36, L22401, doi:10.1029/2009GL039225, 2009

Evolution of shallow groundwater flow systems in areas of degrading permafrost

V. F. Bense,[1] G. Ferguson,[2] and H. Kooi[3]

Received 18 May 2009; revised 15 September 2009; accepted 9 October 2009; published 18 November 2009.

[1] The recent increase in fresh-water discharge during low-flow conditions as observed in many (sub-) Arctic Rivers has been attributed to a reactivation of groundwater flow systems caused by permafrost degradation. Hydrogeological simulations show how groundwater flow conditions in an idealized aquifer system evolve on timescales of decades to centuries in response to climate warming scenarios as progressive lowering of the permafrost table establishes a growing shallow groundwater flow system. Ultimately, disappearance of residual permafrost at depth causes a sudden establishment of deep groundwater flow paths. The projected shifts in groundwater flow conditions drive characteristic non-linear trends in the evolution of increasing groundwater discharge to streams. Although the subsurface distribution of ice will markedly influence the system response, current modeling results suggest that late-stage accelerations in base flow increase of streams and rivers, are to be expected, even if surface air temperatures stabilize at the current levels in the near future.
Citation: Bense, V. F., G. Ferguson, and H. Kooi (2009), Evolution of shallow groundwater flow systems in areas of degrading permafrost, *Geophys. Res. Lett.*, *36*, L22401, doi:10.1029/2009GL039225.

1. Introduction

[2] The Arctic is experiencing an exceptional amount of environmental change today [e.g., *Zhang et al.*, 2008]. Thawing of permafrost, associated with climate warming, is expected to have a profound impact on groundwater flow regimes because, with the disappearance of the confining unit formed by the permafrost, larger groundwater recharge and discharge rates, and deeper flow-paths should develop [e.g., *Michel and van Everdingen*, 1994]. Unfortunately, there is a dearth of supporting groundwater flow data that document such changes in the groundwater flow regime congruent with the degradation of permafrost. There is, however, growing evidence of marked changes in annual and seasonal flows of the large North American and Eurasian rivers [e.g., *Berezovskaya et al.*, 2004] located in (sub-)Arctic regions. Although important questions regarding the significance of inferred trends in flows and the causes of systematic changes in the flows remain especially when hydrological and climatic data are compared from large geographic regions located in both sub-Arctic and Arctic areas [e.g., *Chen and Grasby*, 2009], a number of recent studies have nevertheless provided compelling evidence for increases of the groundwater component contributing to base flow of several major (sub-)Arctic rivers during low-flow conditions in winter, and have related those to permafrost degradation [e.g., *Walvoord and Striegl*, 2007; *St. Jacques and Sauchyn*, 2009].

[3] Here, we investigate the way in which both groundwater flow conditions evolve on timescales of decades to centuries in response to climate warming scenarios impacting an idealized aquifer. Focus is on temporal trends in groundwater discharge rather than discharge magnitudes since the latter are strongly dependent on dimensions of the river catchment.

2. Modeling Approach

[4] We set up a suite of models and calculate transient fluid and heat-flow using FlexPDE software (PDE Solutions, http://www.pdesolutions.com, 2006), employing the finite-element method and which has been used in similar computational studies before [e.g., *Bense and Person*, 2008].

2.1. Governing Equations

[5] The transient hydraulic head (h [m]) field throughout time (t [s]) is calculated assuming:

$$\frac{\rho_w g}{\mu}\nabla\cdot[k\nabla h] = S_s\frac{\partial h}{\partial t} \tag{1}$$

in which ρ_w [kg m^{-3}] is water mass density, μ [kg m^{-1}s^{-1}] is the dynamic viscosity of water and S_s [m^{-1}] is the specific aquifer storage. The left-hand side of equation (1) equals the negative divergence of groundwater discharge. Physical parameter values used are listed in Table 1. Potential variable-density and viscosity effects as function of temperature and/or salinity are not evaluated in the simulations presented here.

[6] Temperature (T [°C]) distributions are calculated, following for example *McKenzie et al.*, [2007], by considering the transient effects of the latent heat associated with melting/freezing which is incorporated in the advection-diffusion equation describing heat-transfer in porous media, as follows:

$$\nabla\cdot[\kappa_a\nabla T] - C_f\vec{q}\cdot\nabla T = C_a\frac{\partial T}{\partial t} + L_i\frac{\partial\theta_w}{\partial t} \tag{2}$$

where C_a [J m^{-3} K^{-1}] is the effective heat capacity of the rock/water/ice mixture and κ_a [W m^{-1} K^{-1}] is the effective

[1]School of Environmental Sciences, University of East Anglia, Norwich, UK.
[2]Department of Earth Sciences, Saint Francis Xavier University, Antigonish, Nova Scotia, Canada.
[3]Faculty of Earth and Life Sciences, VU University, Amsterdam, Netherlands.

0094-8276/09/2009GL039225$05.00

Table 1. Parameter Values Used in the Fluid-Flow and Heat-Transfer Models Discussed in This Study[a]

Parameter	Description	Value	Units
L_i	volumetric latent heat of fusion	$3.03 \cdot 10^8$	J m^{-3}
C_f	volumetric heat capacity of water	$4190 \cdot 10^3$	J m^{-3} K^{-1}
C_i	volumetric heat capacity of ice	$1835 \cdot 10^3$	J m^{-3} K^{-1}
C_s	volumetric heat capacity of sediment grains	$1875 \cdot 10^3$	J m^{-3} K^{-1}
κ_f	thermal conductivity of water	0.54	W m^{-1} K^{-1}
κ_i	thermal conductivity of ice	2.37	W m^{-1} K^{-1}
κ_s	thermal conductivity of sediment grains	4.0	W m^{-1} K^{-1}
S_s	specific storage of the aquifer	10^{-4}	m^{-1}
ρ	fluid density	1000	kg m^{-3}
μ	dynamic viscosity	$1.3 \cdot 10^{-3}$	kg m^{-1}s^{-1}
g	acceleration due to gravity	9.81	m s^{-2}

[a]Thermal property values have been compiled from *Cutler et al.* [2000].

thermal conductivity, and θ_w [dimensionless], is the water-content expressed as a fraction of the total rock volume. The change in water-content from fully water saturated conditions to full permafrost conditions over the thawing interval is prescribed using a smooth function between 0 and −0.5°C. For a given aquifer porosity (n [dimensionless]), expressed as a volumetric fraction, the ice-content (θ_i) follows from the porosity and water-content as $\theta_i = n - \theta_w$ and the solid-grain fraction (θ_s) is equal to $1 - n$. Using these fractions, C_a is calculated as a volumetric weighted mean of the heat capacities of water, ice and solid particles. Effective thermal conductivity, κ_a, is calculated as a weighted geometric mean from the thermal conductivities of rock, water and ice.

2.2. Set-Up and Scenarios

[7] We consider a simple topography-driven groundwater flow system in which groundwater discharge is focused in a central topographic low from flanking recharge areas (Figure 1a). Groundwater flow is driven by a water table gradient of $4 \cdot 10^{-4}$. Although trends in predicted groundwater discharge are largely independent of chosen model scales, the drainage density of the adopted geometry of km^{-1} is well within the range of values for subarctic landscapes [*Luoto*, 2007]. Hydraulic head along the surface is fixed and is assumed to closely coincide with the topography and the water table. We thus assume that there is always enough precipitation excess to maintain the water table at this maximum position. The base and sides of the model are closed for fluid flow. A uniform heat flow density of 65 mW/m^2 is prescribed at the base representing geothermal heat production while the sides of the model are closed for heat exchange. Surface temperature is considered to be uniform.

[8] Three different scenarios are considered (I–III; Figure 1b), corresponding to an initial surface temperature of −2, −1.5, and −1°C respectively. This corresponds to initial permafrost thicknesses of roughly 85, 55 and 30 m. Each starting condition represents a steady-state for both fluid- and heat-flow. The seasonally varying surface temperature is not considered here as the active layer thickness which will develop during summer months when the surface temperatures rise above freezing will rarely exceed several meters [e.g., *Anisimov et al.*, 1997], which is too thin to significantly impact our modeling results. In all three scenarios the average seasonal surface temperature is increased by three degrees Celsius over 100 years (Figure 1b), in agreement with average model predictions [*Meehl et al.*, 2007]. However, these are probably conservative warming scenarios with regards to Arctic regions as numerical simulations summarized in *Meehl et al.*, [2007] show the potential for warming over the Arctic of >5°C for the coming century. After this period of warming temperature is kept constant and the models are run for a further 1100 years so that total model time is 1200 years. These scenarios are applied for three different values of unfrozen aquifer permeability, i.e., $4 \cdot 10^{-14}$, $2 \cdot 10^{-13}$, and $1 \cdot 10^{-12}$ m^2, which are within the range of shallow sedimentary aquifers [e.g., *Freeze and Cherry*, 1979] underlying many catchments in areas where currently permafrost conditions exist. These values are representing the aquifer's permeability in the horizontal direction (k_x) while the effect of sedimentary stratification is mimicked by setting the vertical component of permeability (k_y) to be one order of magnitude lower than k_x. In the simulations aquifer porosity is set to 0.25, but for one model run we varied the aquifer porosity between 0.175 and 0.325. In these scenarios, under permafrost free conditions groundwater recharge never exceeds ~60 mm/year which is within the range for present-day climatic conditions in permafrost-free lowland areas in the sub-Arctic [e.g., *Smerdon et al.*, 2008]. Although we note that the homogeneous permeability structure of the aquifer will not be applicable to aquifers directly within fractured igneous and metamorphic basement rocks, for example, those found across much of the Canadian Shield, a major portion of the estimated permafrost volume is located in (sub-)Arctic regions that are underlain by sedimentary rocks or thick unconsolidated deposits [e.g., *Zhang et al.*, 2000].

[9] Where all pore fluids are frozen ($\theta_w = 0$) permeability will approach effectively zero. Experimental data (Figure 1c) suggest that the permeability reduction (relative permeability), k_{rw}, as function of water-saturation state ($p_w = \frac{\theta_w}{n}$), can be described by:

$$k_{rw} = \frac{{p_w}^4}{\left(1 + (1 - p_w)^{0.5}\right)^2} \tag{3}$$

[10] Equation 3 is incorporated into the modeling routine to represent the temporally varying permeability distribution over the course of the simulation. A lower limit is set for p_w at ~2% resulting in a permeability reduction of approximately eight orders of magnitude. Total groundwater discharge across the upper boundary of the model domain, Q_b [m^3/s/m], is concentrated in the lower areas of the

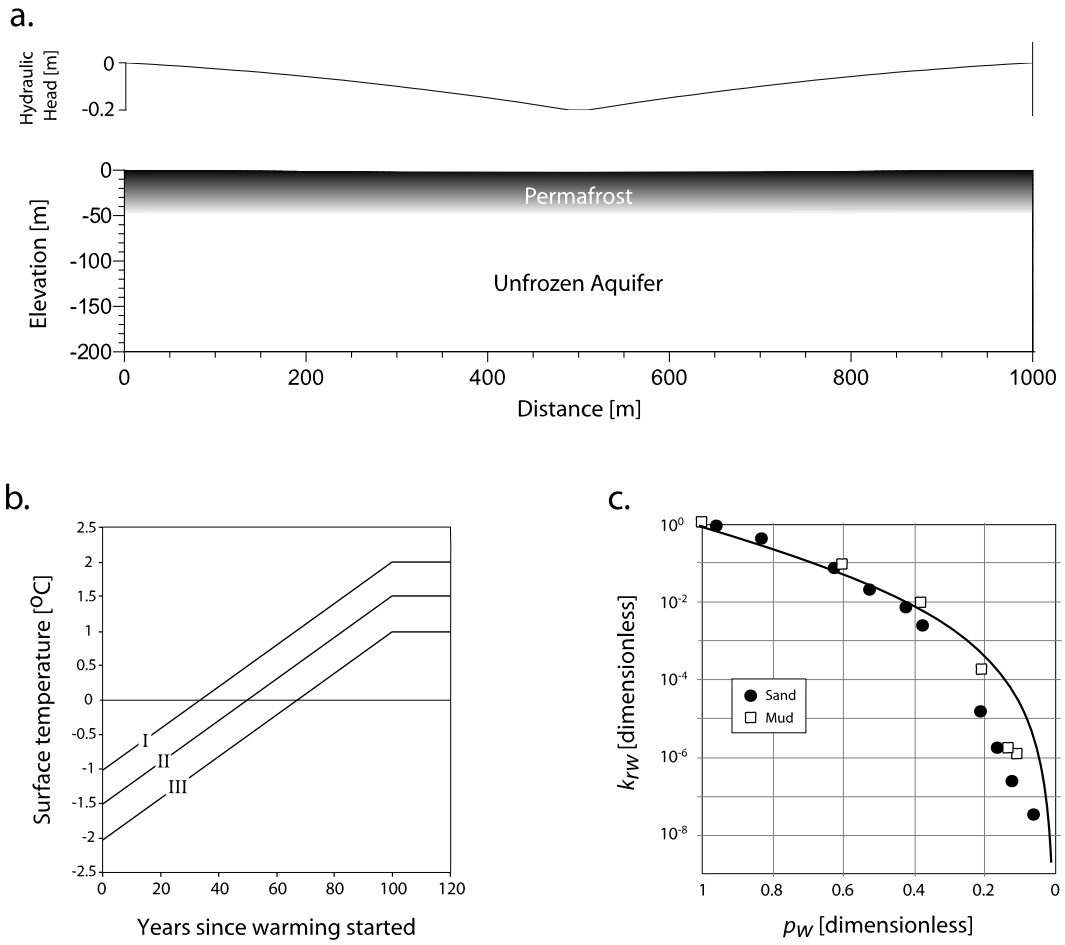

Figure 1. (a) Model domain used in the simulations showing the shape of the imposed water table at the surface; note that the vertical scale is exaggerated in order to make the shape of the water table visible. The unclassified shaded area indicates extent of permafrost for a steady surface temperature of −1°C. (b) Three scenarios of warming (I–III) are considered in this study. (c) Data showing reduction of permeability (k_{rw}) as function of water saturation (p_w) for different sediment types [*Kleinberg and Griffin*, 2005]. The solid curve is a fit of the data via equation (3).

topography, and represents the groundwater contribution to stream flow from wetland and riparian zones around the main river channel plus direct groundwater discharge through the stream bed.

3. Results

[11] Figure 2 shows the evolution of the groundwater flow system for modeling scenario II and $k_x = 1 \cdot 10^{-12}$ m^2. At the end of the episode of surface warming ($t = 100$ years), a shallow aquifer has formed above the permafrost table. At this time, the capacity of the upper aquifer is limited to transport groundwater while the remaining permafrost at depth prevents any regional circulation of groundwater. At $t = 300$ years, the upper aquifer has doubled in thickness. Only after t = 500 years permafrost has become so much reduced that regional-scale flow paths will become significant.

[12] The evolution of groundwater discharge (Figure 3) is understood from the spatiotemporal patterns in the evolution of aquifer structure. At the initial stages of the simulations groundwater outflow is negligible as permeability in the aquifer in the frozen state is very small (Figure 1). During the first period over which surface warming is occurring (grey areas in Figure 3) for all models groundwater discharge is approximately linearly increasing with growing thickness of the shallow aquifer. At later time, the patterns for the different scenarios start to diverge, reflecting the fact that it takes longer to melt all permafrost and to reach associated steady-state flow conditions for larger initial permafrost thickness (scenario I → III). For all scenarios the rate of increase in groundwater outflow then declines, after which acceleration takes place, before a steady-state situation is reached. The late-time acceleration of discharge increase is linked to the final phases of permafrost degradation when remnant deep permafrost disappears and deep flow patterns are established (Figure 2c). For different aquifer permeabilities the temporal patterns described above remain the same while the absolute value of groundwater outflow directly scales with permeability. For larger porosities permafrost degradation is delayed as more heat is needed to fully thaw the ice occupying the larger amount of pore space (Figure 2d).

4. Discussion and Conclusion

[13] The present results provide, to our knowledge, the first model predictions of the way in which permafrost-

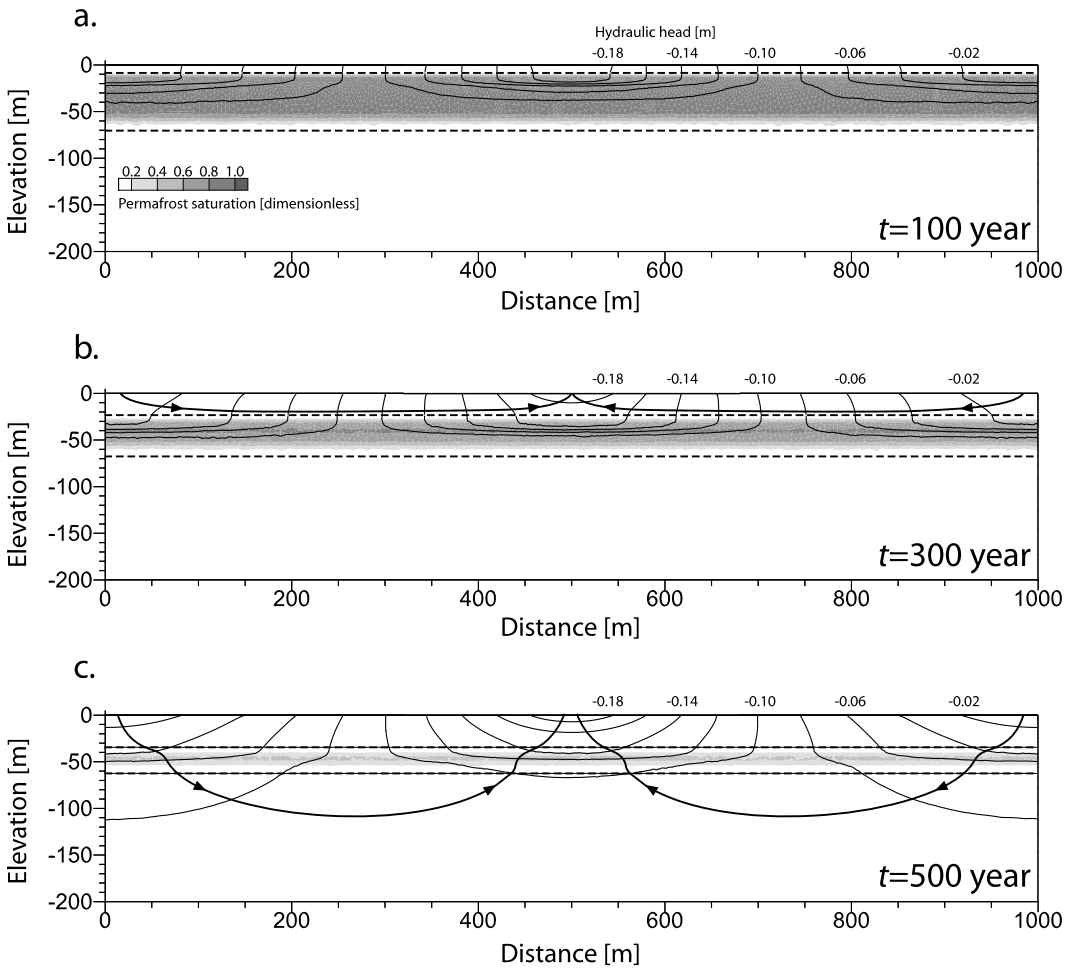

Figure 2. The simulated transient hydraulic-head field for modeling scenario II and $k_x = 1 \cdot 10^{-12}$ m^2, at t = (a) 100 years, (b) 300 years, and (c) 500 years. The dashed line indicates the position of the 0°C isotherm. Solid contour lines depict hydraulic head in meters. Groundwater flow lines representative of the groundwater flow conditions are shown for Figures 2b and 2c. Grey shading shows the extent of permafrost saturation (1-p_w).

covered and therefore dormant groundwater flow systems are re-activated as a function of permafrost thawing, forced by a projected magnitude surface warming of 3°C over one century. Our results show that even if surface air temperatures stabilize at the current levels in the near future, it is likely that substantial increases in groundwater discharge over the next few centuries will occur, in addition to changes in stream flow resulting from other climatic factors, such as shifts in precipitation regimes across the Arctic.

[14] The simulations presented here highlight nonlinearity in the increase in total groundwater discharge to streams and rivers and marked delays in discharge response, which are positively linked to initial permafrost thickness and aquifer ice-content. One of the most intriguing, robust predictions of the current set of experiments is a late-stage acceleration of groundwater discharge associated with removal of residual permafrost. Although the current simulations demonstrate first-order controls and behaviors, further modeling is required to explore the influence of more detailed surface temperature distributions, for example related to the presence of surface water, vegetation, topography and snow cover, factors which exert a considerable control on lateral variability in subsurface ice content [*Smith*, 1975]. Additionally, the role of water table adjustments and vadose zone processes and more complex aquifer architecture will need to be quantified.

[15] Our modeling results are in qualitative agreement with the recently inferred increases in winter low flows of several (sub-)Arctic rivers, as in most of this region, at least 1°C warming has already occurred over the last half of the 20th century [e.g., *Serreze et al.*, 2000], while in large parts of the (sub-)Arctic regions warming started already during the last half of the 19th century [e.g., *Douglas et al.*, 1994]. This paper's set of models suggest that most of the base flow and base flow increase is linked to shallow, supra-permafrost groundwater systems. This would particularly apply to high latitudes, as our simulations, in essence, start with continuous permafrost conditions. As relatively thick and continuous supra-permafrost aquifer systems (taliks) are unlikely to have already developed at present, but considerable winter discharge has been reported, our modeling may well underestimate the groundwater component in streams under relatively cold climatic conditions. On the other hand winter stream discharge of Arctic rivers within continuous permafrost areas could potentially originate mostly from other sources than groundwater discharge such

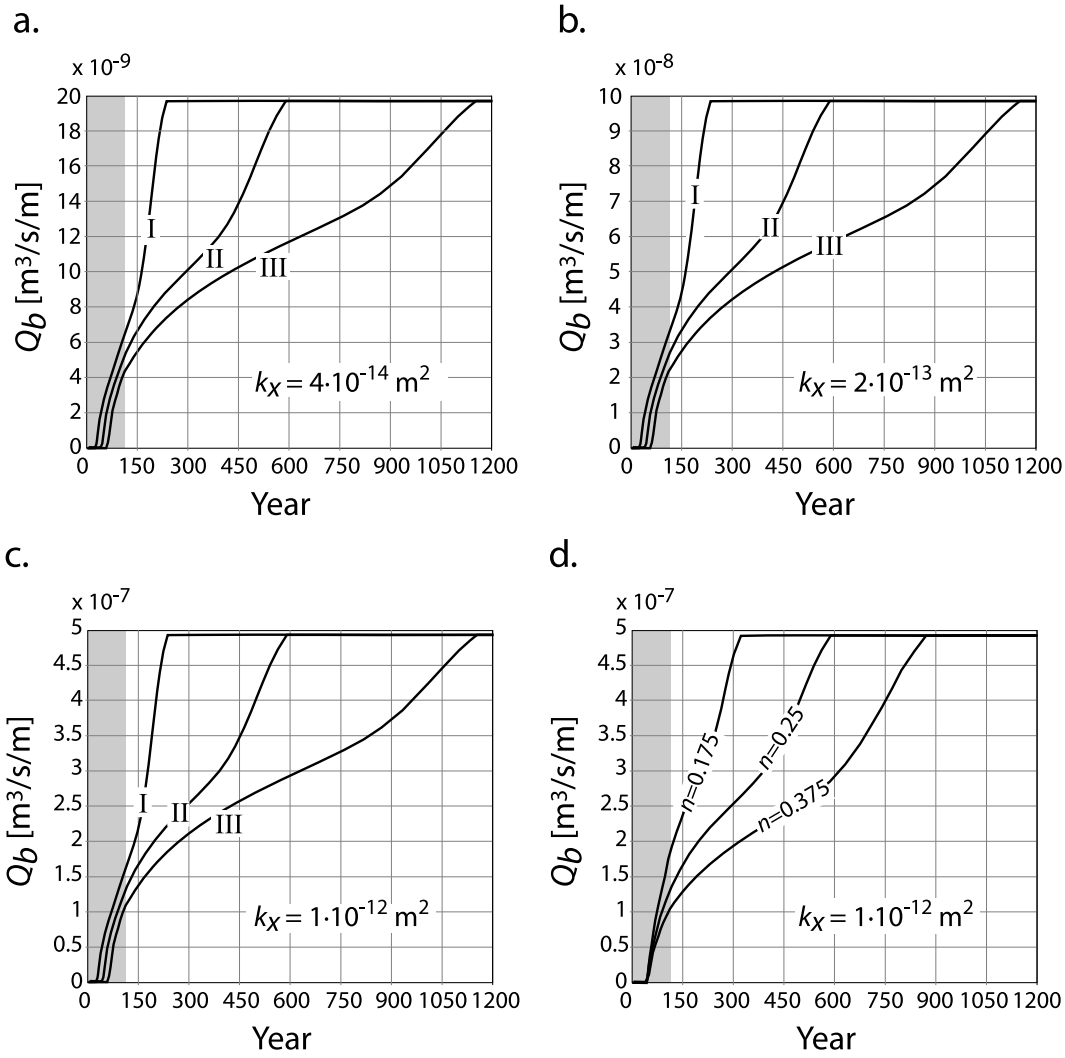

Figure 3. (a–c) Development of groundwater discharge integrated across the upper model boundary (Q_b) for surface warming scenario I–III and a range of aquifer permeabilities, k_x. (d) The calculated evolution of groundwater discharge across the top of the modeling domain for surface warming scenario II and an aquifer permeability of 10^{-12} m^2 for different values of aquifer porosity, n. The shaded area indicates the warming phase during the first 100 years of the simulation.

as unfrozen lakes or patches of land where permafrost is discontinuous due to surface conditions. Nevertheless, detection and separation of shallow and deep groundwater components in present Arctic streams will provide crucial data to constrain the employed modeling approach.

[16] We anticipate that the approach and insights provided here will begin to aid in establishing process-based projections of further increases of groundwater inflow to streams and rivers over the coming centuries via the development of algorithms allowing the coupling of groundwater flow and surface hydrological and climate models in (sub-)Arctic regions. A well-founded understanding of the recent climate histories of different parts of the (sub-)Arctic regions will in this process become of paramount importance to differentiate between the stages in the evolution of groundwater discharge various regions can be expected to be in, allowing a more refined interpretation of hydrological field data from these areas.

[17] **Acknowledgments.** Steve Grasby and two anonymous reviewers are thanked for constructive comments which contributed to the quality of this letter.

References

Anisimov, O. A., N. I. Shiklomanov, and F. E. Nelson (1997), Global warming and active-layer thickness: Results from transient general circulation models, *Global Planet. Change*, *15*, 61–77.

Bense, V., and M. Person (2008), Transient hydrodynamics in inter-cratonic basins during glacial cycles, *J. Geophys. Res.*, *113*, F04005, doi:10.1029/2007JF000969.

Berezovskaya, S., D. Yang, and D. Kane (2004), Compatibility analysis of precipitation and runoff trends over the large Siberian watersheds, *Geophys. Res. Lett.*, *31*, L21502, doi:10.1029/2004GL021277.

Chen, Z., and S. E. Grasby (2009), Impact of decadal and century-scale oscillations on hydroclimate trend analyses, *J. Hydrol.*, *365*, 122–133, doi:10.1016/j.jhydrol.2008.11.031.

Cutler, P. M., D. R. MacAyeal, D. M. Mickelson, B. R. Parizek, and P. M. Colgan (2000), A numerical investigation of ice-lobe-permafrost interaction around the southern Laurentide ice sheet, *J. Glaciol.*, *46*, 311–325.

Douglas, M. S. V., W. Smol, and J. P. Blake Jr. (1994), Marked post-18th century environmental change in high-arctic ecosystems, *Science*, *266*, 416–418.

Freeze, R. A., and J. A. Cherry (1979), *Groundwater*, 1st ed., Prentice-Hall, London.

Kleinberg, R., and D. Griffin (2005), NMR measurements of permafrost: Unfrozen water assay, pore-scale distribution of ice, and hydraulic permeability of sediments, *Cold Reg. Science Technol.*, *42*, 63–77.

Luoto, M. (2007), New insights into factors controlling drainage density in subarctic landscapes, *Arct. Antarct. Alp. Res.*, *39*, 117–126.

McKenzie, J. M., C. I. Voss, and D. I. Siegel (2007), Groundwater flow with energy transport and water-ice phase change: Numerical simulations, benchmarks, and application to freezing in peat bogs, *Adv. Water Resour.*, *30*, 966–983, doi:10.1016/j.advwatres.2006.08.008.

Meehl, G., et al. (2007), Global climate projections, in *Climate Change 2007: The Physical Science Basis. Contributaion of Working Group I to the Fourth Assessment Report of the Intergovernmental Panel on Climate Change*, edited by S. Solomon et al., chap. 10, 747–846, Cambridge Univ. Press, Cambridge, U. K.

Michel, F. A., and R. O. van Everdingen (1994), Changes in hydrogeologic regimes in permafrost regions due to climatic change, *Permafrost Periglacial Processes*, *5*, 191–195.

Serreze, M. C., et al. (2000), Observational evidence of recent change in the northern high-latitude environment, *Clim. Change*, *46*, 159–207.

Smerdon, B. D., C. A. Mendoza, and K. J. Devito (2008), Influence of subhumid climate and water table depth on groundwater recharge in shallow outwash aquifers, *Water Resour. Res.*, *44*, W08427, doi:10.1029/2007WR005950.

Smith, M. (1975), Microclimatic influences on ground temperatures and permafrost distribution, Mackenzie Delta, Northwest Territories, *Can. J. Earth Sci.*, *12*, 1421–1438.

St. Jacques, J.-M., and D. J. Sauchyn (2009), Increasing winter baseflow and mean annual streamflow from possible permafrost thawing in the Northwest Territories, Canada, *Geophys. Res. Lett.*, *36*, L01401, doi:10.1029/2008GL035822.

Walvoord, M., and R. Striegl (2007), Increased groundwater to stream discharge from permafrost thawing in the Yukon River Basin: Potential impacts on lateral export of carbon and nitrogen, *Geophys. Res. Lett.*, *34*, L12402, doi:10.1029/2007GL030216.

Zhang, T., J. A. Heginbottom, R. G. Barry, and J. Brown (2000), Further statistics on the distribution of permafrost and ground ice in the Northern Hemisphere, *Polar Geogr.*, *24*, 126–131.

Zhang, Y., W. Chen, and D. W. Riseborough (2008), Disequilibrium response of permafrost thaw to climate warming in Canada over 1850–2100, *Geophys. Res. Lett.*, *35*, L02502, doi:10.1029/2007GL032117.

V. F. Bense, School of Environmental Sciences, University of East Anglia, Norwich NR4 7TJ, UK. (v.bense@uea.ac.uk)

G. Ferguson, Department of Earth Sciences, Saint Francis Xavier University, Antigonish, NS B2G 2W5, Canada.

H. Kooi, Faculty of Earth and Life Sciences, VU University Amsterdam, NL-1081 HV Amsterdam, Netherlands.